Proc. Natl. Acad. Sci. USA
Vol. 88, pp. 4391–4395, May 1991
Neurobiology

Ion channels in transit: Voltage-gated Na and K channels in axoplasmic organelles of the squid *Loligo pealei*

(squid giant axon/axoplasmic transport/integral membrane proteins)

WILLIAM F. WONDERLIN* AND ROBERT J. FRENCH

Department of Medical Physiology and Neuroscience Research Group, University of Calgary, Calgary, AB, Canada T2N 4N1

Communicated by Clay M. Armstrong, February 25, 1991 (received for review July 14, 1990)

ABSTRACT **Ion channels that give rise to the excitable properties of the neuronal plasma membrane are synthesized, transported, and degraded in cytoplasmic organelles. To determine whether plasma membrane ion channels from these organelles could be physiologically activated, we extruded axoplasm from squid giant axons, dissociated organelles from the cytoskeletal matrix, and fused the free organelles with planar lipid bilayers. Three classes of ion channels normally associated with the plasma membrane were identified based on conductance, selectivity, and gating properties determined from steady-state single-channel recordings: (*i*) voltage-dependent Na channels, (*ii*) voltage-dependent delayed rectifier K channels, and (*iii*) large, voltage-independent K channels. The identity of the delayed rectifier channels was confirmed by reconstructing the time course of activation from single-channel responses to depolarizing voltage steps applied across the bilayer. These observations suggest that several classes of plasma membrane ion channels are transported in cytoplasmic organelles in physiologically active forms.**

Ion channels in the plasma membrane of neurons provide the molecular basis for the voltage-dependent changes in ion permeability that underlie electrical excitability (1). The lifetime of these integral membrane proteins includes, in addition to their residence in the plasma membrane, periods during which they are synthesized, transported, and degraded in several classes of cytoplasmic organelles (2). For several types of plasma membrane ion channels, biochemical and molecular biological approaches have revealed important structural modifications that occur during the stepwise processing of these channels by different organelles (3). From these studies, it seems likely that the structure of the channels as they reside in various classes of organelles might differ from their native structure *in situ* in the plasma membrane. If plasma membrane channels could be obtained from organelles, might such structural variations be reflected in altered physiological properties? The feasibility of studying this intracellular pool of channels hinges on the fundamental question of whether these channels are "silent" (i.e., nonconducting) or can be physiologically activated and studied by single-channel recording methods.

To address this question, we have sought to identify ion channels in organelles from the axoplasm of the giant axon that are homologous to channels in the plasma membrane of the squid giant axon. The squid giant axon was chosen for our study because (*i*) axoplasm can be obtained by roller extrusion, with little likelihood of contamination by plasma membrane, and (*ii*) its repertoire of plasma membrane channels consists of a few, well-characterized types, which facilitates identification of homologous channels present in organelles. Each giant axon is formed by the anastomosis of small axons projecting from hundreds of cell bodies located in the giant fiber lobe of the stellate ganglion (4). In neurons, protein synthesis is generally restricted to the cell bodies (5), and this appears to be true for the syncytial giant axon. The organelles involved in protein synthesis and degradation are found only in cell bodies in the giant fiber lobe, whereas, in the giant axon, the organelles are limited to mitochondria, smooth endoplasmic reticulum, and vesicles undergoing bidirectional fast axonal transport, shuttling proteins and other membrane constitutents between the cell bodies and the axolemma and nerve terminal (6). As a result of this segregation, plasma membrane ion channels found in organelles sampled from the axoplasm of the giant axon are probably either (*i*) in transport to the axolemma or nerve terminal, having completed processing in the Golgi, or (*ii*) being returned to the cell bodies for degradation, following removal from the plasma membrane. Our goal was to study single, plasma membrane ion channels obtained from these transport organelles. The likelihood of finding plasma membrane ion channels in transport organelles seemed high because cultured cell bodies from the giant fiber lobe of the stellate ganglion are capable of high rates of Na-channel synthesis, and these channels are transported to the plasma membrane via fast axoplasmic transport (7).

METHODS

The method for dissociation of organelles was adapted from previous studies of organelle tranport (8, 9). Giant axons were removed from *Loligo pealei* captured at the Marine Biological Laboratory (Woods Hole, MA). Axoplasm was collected by the roller extrusion method (10). Sections of giant axon (5–7 cm long) were removed, stored, and cleaned in Ca^{2+}-free artificial seawater. The adherent connective tissue and small nerve fibers were removed thoroughly for a length of ≈1 cm from the proximal end of the axon. The giant axon was laid on a piece of filter paper and the axoplasm extruded onto a piece of Parafilm, rolling from the distal end to within ≈5 mm of the proximal end. The cytoskeletal matrix of the axoplasm was dissolved by addition of KI buffer (0.6 M potassium iodide/10 mM $MgCl_2$/5 mM EGTA/1 mM phenylmethylsulfonyl fluoride/100 μg of soybean trypsin inhibitor per ml/10 mM Hepes, pH 7.4; 4–10 μl per cm of axon length) to the extrudate, followed by trituration of the pooled, KI-treated axoplasm from 4–20 axons. The extrudate was diluted 1:5 in 1 M sucrose buffer (1 mM EDTA/1 mM phenylmethylsulfonyl fluoride, 100 μg of soybean trypsin inhibitor per ml/10 mM Hepes, pH 7.4) and centrifuged for 5 min at 1310 × *g*. The supernatant was removed and either stored on ice for immediate use or frozen at −80°C, where it remained viable for 4–8 weeks. Few organelles were observed when the supernatant was viewed with a standard light microscope (Zeiss Axiophot, DIC; ×2000), but video-enhanced microscopy (Hamamatsu SIT camera) revealed the

The publication costs of this article were defrayed in part by page charge payment. This article must therefore be hereby marked "*advertisement*" in accordance with 18 U.S.C. §1734 solely to indicate this fact.

Abbreviation: BTX, batrachotoxin.

*Present address: Department of Pharmacology and Toxicology, West Virginia University, Morgantown, WV 26506.

presence of many organelles, most of which were less than ≈0.5 μm in diameter.

Dissociated organelles were fused with a planar lipid bilayer, enabling single-channel recordings after incorporation of ion channels into the bilayer membrane. Planar bilayers were painted from synthetic 1-palmitoyl-2-oleoyl phosphatidylethanolamine: 1-palmitoyl-2-oleoyl phosphatidylcholine (Avanti Polar Lipids) in an 80:20 or 90:10 ratio dissolved in decane (33 mg/ml). Bilayers were formed on holes (60–120 μm diameter) in polyethylene or polystyrene cups. The total input capacitance ranged from ≈20 to 50 pF. Recording solutions contained 10 mM Hepes (pH 7.0), 100 μM EGTA, and the acetate salts of either Na^+ or K^+. Acetate salts were used to minimize background currents. The dissociated axoplasm was pressure applied to the bilayer with a hand-held glass pipette. Single-channel currents were recorded with an Axopatch-1B amplifier with a CV-3 headstage modified as described (11). Liquid junction potentials were calculated by Henderson's equation (12) and subtracted from command voltages. Experiments were performed at room temperature, 22°C–24°C.

Significant contamination of the axoplasm preparation by vesicles formed from plasma membrane is unlikely because, as reviewed in ref. 13, roller extrusion (*i*) removes axoplasm only from the core of the axon, leaving intact the plasma membrane and a thin layer of axoplasm (≈10 μm thick) under the plasma membrane and (*ii*) does not appear to damage the plasma membrane, as excitability is preserved and the axon does not become permeable to normally impermeant radiolabeled molecules. Also, we were unsuccessful when we attempted to incorporate ion channels from axolemmal vesicles made by homogenizing the giant axon and sheath after extrusion of the axoplasm, indicating that incorporation from axoplasmic organelles is considerably more likely than from axolemmal membrane vesicles.

RESULTS

Single Na channels were studied in the presence of batrachotoxin (BTX; 750 nM), which removes both fast and slow inactivation and enables steady-state recording (Fig. 1*A*). The steep, voltage-dependent increase in fractional open time (F_o) between −100 and −40 mV (Fig. 1*B*), linear current–voltage relationships (Fig. 1*C*), and an average single-channel conductance of 16.1 ± 0.5 pS (mean ± SEM) in symmetric 200 mM NaOAc (n = 4) closely resemble those of BTX-modified, voltage-gated axolemmal Na channels in the giant axon of the squid *L. pealei* (15) and the squid optic nerve [from the Venezuelan squid, *Sepiotheutis sepioidea* (14) and from *L. pealei* (unpublished observations)].

Two types of K channels were observed. The first, small-conductance, type resembled a class of K channel that is thought to underlie the macroscopic delayed rectifier current in the axolemma of the giant axon (16, 17) and the somal membrane of dissociated giant fiber lobe neurons (18). This channel exhibited bursts of brief openings (Fig. 2 *A* and *B*) and a steep, voltage-dependent increase in F_o between −100 and −60 mV (Fig. 2*C*). A Boltzmann function was fitted to the activation curve for each experiment (Fig. 2*C*). The channels exhibited a maximal activation of $F_o \approx 0.3$, with half-maximal activation at −63.0 ± 2.7 mV (n = 7; range, −47 to −76 mV), and an apparent gating charge for records with only one active channel of 3.91 ± 0.16 e (n = 4). Slow inactivation was also evident in the steady-state records as long closures (>2 sec) at these potentials. The inactivation could be removed by holding the voltage at −90 or −100 mV for a few seconds.

The activity of the axoplasmic small conductance K channels differed quantitatively from typical plasma membrane delayed rectifier K channels in that the steady-state activation curve was shifted in a negative direction by ≈50 mV

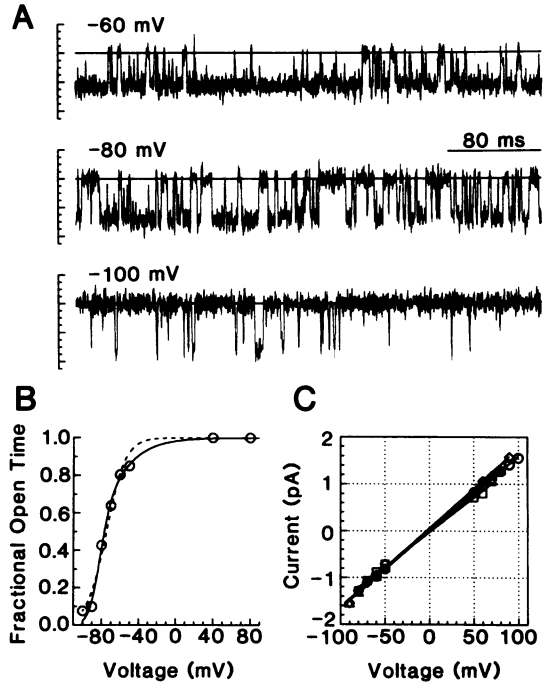

FIG. 1. (*A*) Steady-state activity of a single, BTX-modified Na channel (low-pass Gaussian digitally filtered at 1 kHz, 200 mM $NaOAc_{out}$/150 mM KCl_{in}; large tic interval is 1 pA). The channel current fluctuates between the closed level (solid line) and the unitary current amplitude, with little evidence of conductance substates. (*B*) The fractional open time (F_o) was calculated for steady-state records from the experiment shown in *A*. The voltage dependence of the activation process was examined by fitting the activation curve with one-component (dotted line) and two-component (solid line) Boltzmann functions. An improved fit of the upper part of the curve (F_o > 0.7) was generally obtained with addition of the second component, as noted by Behrens and coworkers (14), for BTX-modified Na channels in the optic nerve of the squid. This is consistent with the idea that the channel has at least two kinetically distinct closed states. The parameter values for the best fit were −78 and −91 mV for the midpoints of the two components and 3.84 and 1.13 e for the respective apparent gating charges. (*C*) Single-channel *I–V* relations from four channels in symmetric 200 mM NaOAc.

(19–21). Two factors might contribute to this shift. First, the absence of external divalent cations in our recording solutions might make the surface potential at the external end of the channel more negative. A negative shift of 20–25 mV has been observed for axolemmal delayed rectifier channels on reducing the divalent ion concentrations from seawater levels (≈60 mM) to zero (19). Second, a positive shift of 25–30 mV has been reported for axolemmal delayed rectifier channels following a change from dephosphorylating to phosphorylating conditions (22). The small K channels that we observed might represent an unphosphorylated form.

Analysis of the *I–V* relations of the small K channel was hindered by filtering of the predominantly brief channel openings and closures. The rapidly fluctuating, filtered current rarely reached a stable level that could be clearly and repeatedly measured by cursor. The open-level peak of the all-points current amplitude histogram was distorted by the flickering; its standard deviation was broadened by a factor of 2–4 relative to that of the baseline component (Fig. 3*A*). When compared to the raw data record, the open-channel peak generally underestimated the largest observed open-channel level (Fig. 3*B*). Because of these difficulties in measuring the open-channel current amplitude, we used an alternative, empirical method for analysis of the current amplitude histogram. Under the conditions that: (*i*) there are at least a few openings to the fully open level in the record,

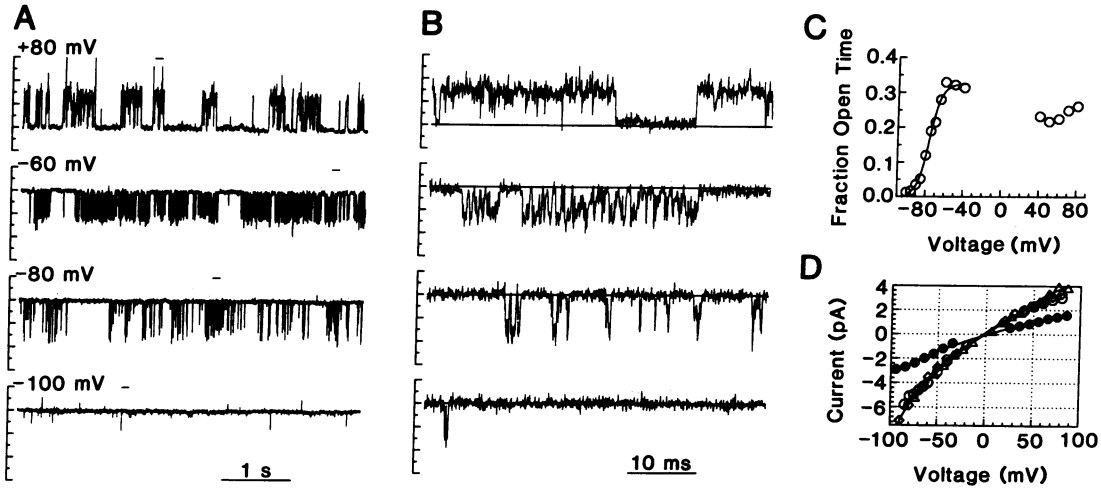

FIG. 2. (*A*) Steady-state activity of a single, voltage-dependent K channel (digitally filtered at 1 kHz, symmetric 500 mM KOAc; large tic interval is 2 pA). The channel openings were grouped in bursts, with the burst duration increasing and the interburst interval decreasing with depolarization between −100 and −60 mV. There is an occasional, very brief opening of a large K channel in the background (e.g., record at +80 mV). (*B*) The segments of records in *A* marked by horizontal bars are shown with expanded time scale and wider bandwidth (2.5 kHz). At negative potentials, the intraburst gating is marked by very rapid flickering, and the current amplitude very rarely reaches the maximum open-channel amplitude. The flickering is less prominent at positive potentials. (*C*) F_o plotted versus membrane potential for the experiment shown in *A*. F_o was calculated from the relative areas under the peaks in all-points current amplitude histograms constructed from steady-state records. The fractional open time increased steeply between −100 and −60 mV and generally exhibited a variable decrease in fractional open time at more positive potentials, probably as a result of an increase in slow inactivation. The smooth curve is a single-component Boltzmann function fitted to the data over the voltage range of −100 to −40 mV. For this channel, the midpoint of the activation curve was −75.5 mV, and the apparent gating charge was 3.93 *e*. (*D*) Single-channel *I–V* relations measured from steady-state recordings for four single-channel experiments in symmetric K^+ solutions. The open and solid symbols denote data recorded in 500 and 200 mM KOAc, respectively.

and (*ii*) the distortion of the histogram produced by the flickering is mostly limited to the interval between the mean baseline and open-channel current levels, the distributions of points in the tails beyond this interval should be similar, with the same standard deviation (which is determined by the baseline noise) and differing only in mean value and area. Both of these conditions appear to be met for our small K-channel data. In particular, because most of the filtered brief openings (Fig. 3*B*, cursor b) do not even approach the full amplitude, the tail of the broad distribution b does not appreciably extend beyond the mean of the fully open level a (Fig. 3*A*). For each all-points current amplitude histogram, we fitted the foot of the tail of the open level with a Gaussian curve that had the same standard deviation as the baseline noise (Fig. 3). The Gaussian curve was positioned along the current axis and its amplitude was scaled to maximize the length of the tail over which the two curves superimposed. The mean of this Gaussian curve was taken as an estimate of the open-channel current level. The appropriate positioning was generally unambiguous, and this method provided a consistently good estimate of the open-channel current amplitude, when compared with the raw data record. The greater accuracy of this method was further supported by analysis of simulated data records. For example, the opening and closing rates for a closed–closed–open kinetic scheme were selected such that the average open time was 40 μsec (i.e., a closing rate constant of 25 kHz) and the steady-state probability of the channel being open was ≈7%. When a current-amplitude histogram was constructed from this simulated record filtered at 5 kHz, the peak of the histogram and the Gaussian fit to the tail underestimated the true unitary current amplitude by 20% and 6%, respectively.

When open-channel current amplitudes were measured by the tail-fit method, the *I–V* relationship was nearly linear (Fig. 2*D*), with some inward rectification. The slope conductance at 0 mV in symmetric KOAc solutions was 24 pS (200 mM; $n = 1$) and 49.1 ± 1.8 pS (500 mM; $n = 3$). The channels were selective for K^+ over Na^+. When recorded under biionic conditions (200 or 500 mM K^+ and Na^+, both orien-

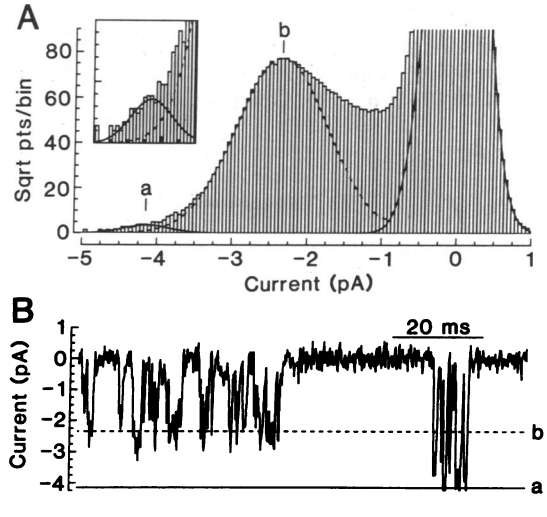

FIG. 3. Method of Gaussian tail-fitting of a current amplitude histogram. (*A*) The steady-state current recorded at −60 mV (digitally filtered at 1.56 kHz, symmetric 500 mM KOAc) was digitized and binned (20 bins per pA; ordinate, square root of number of points per bin) to form an all-points current–amplitude histogram. The histogram contained two peaks, a large peak at the closed-channel current level and a smaller, broader peak near the middle of the distribution. The dashed line is a Gaussian fit by eye to the open-channel peak, indicated by b, with a standard deviation about twice that of the baseline noise. The solid line is a two-component fit in which the open-channel component, indicated by a, was fitted with its standard deviation equal to that of the baseline noise and its amplitude and area adjusted to give the best fit to the foot of the tail of the histogram. (*Inset*) An expanded view of this component. (*B*) A rare, full opening of the K channel in the record from which the histogram in *A* was constructed (filtered at 1.56 kHz). The current levels corresponding to the fitted peaks marked by a and b in *A* are indicated by the horizontal cursors. The b level underestimates the open-channel current level because the points near this peak are from poorly resolved, rapid openings and closures. The a level is less sensitive to the presence of flickering and provides a better approximation to the largest open-channel current level.

tations), the single-channel currents were observed to extrapolate toward a relatively large (30–78 mV) reversal potential, but a more detailed analysis was not possible because reversed currents generally could not be recorded. The difficulty in reversing the currents resulted, in part, from the voltage-dependent decrease in fractional open time, even at positive potentials.

The small-conductance K channel could be deactivated by holding at −100 mV and then activated by brief depolarizing steps to various test potentials (Fig. 4*A*). Recently developed recording techniques (11) allowed us to obtain, from ensembles of step-activated currents, averaged records that exhibited a sigmoidal onset (Fig. 4*A*). These averaged records were analyzed by using a modified Hodgkin–Huxley formalism (23). The time constant of activation was voltage dependent (Fig. 4*C*) with a maximum value occurring between −65 and −70 mV. For each channel, the maximum time constant of activation occurred within 5–10 mV, in either direction, of the midpoint voltage of the steady-state activation curve. (A strict n^4 model predicts that the time constant peak should be ≈12 mV to the left of the activation midpoint for our estimate of the gating charge.) In addition to the slow inactivation described above, we observed a more rapid inactivation during voltage steps to potentials more positive than −60 mV. Although inactivation of delayed rectifier K currents is not part of the original Hodgkin–Huxley formalism, inactivation of both macroscopic and single-channel delayed rectifier K currents has been reported (18, 24). We fitted the inactivation as a single-exponential decay toward zero current at infinite time. The apparent time constant of inactivation was voltage dependent, with an *e*-fold decrease for each 4.8-mV depolarization (Fig. 4*D*).

The second, larger-conductance, type of K channel exhibited voltage-independent gating and a very low fractional open time (<0.01) (Fig. 5*A*). Openings were typically infrequent and brief. The slope conductances at 0 mV in symmetric 200 and 500 mM KOAc were 50 and 153 pS, respectively (Fig. 5*B*). Occasionally, this large K channel opened in long bursts of high activity (Fig. 5*C*). It resembled a K channel observed in patch-clamp recordings from the axolemma of the squid giant axon (ref. 16; their 40-pS channel) in its relative conductance and in showing both low- and high-activity modes. However, we could not confirm this homology because the rare occurrence of the high-activity mode in our study prevented us from determining whether the axoplasmic large K channel exhibited voltage-dependent gating similar to that of the high-activity mode of the axolemmal channel. In the axolemma, the low-activity and high-activity modes are typically observed under dephosphorylating and phosphorylating conditions, respectively (25).

DISCUSSION

What is the intraaxonal source of the axoplasmic Na and K channels? We suggest that the channels were incorporated from membrane vesicles, probably transport organelles. Although a cytosolic, soluble saxitoxin receptor has been reported in vertebrate muscle, it is probably not the voltage-gated Na channel (26). It seems likely that the channels we observed are present subcellularly in organelle membranes, as reported for the primary subunit of the Na channel from rat brain (27). Incorporation by fusion of channel-containing organelles with the lipid bilayer best accounts for the relative ease of incorporation into an artificial bilayer and, in multichannel incorporations, the identical orientation of all channels. During their transport in organelles either prior to fusion into the axolemma or after endocytosis from the axolemma, plasma membrane channels should be oriented nonrandomly, with the end of the channel that normally faces the cytoplasmic side of the axolemma also facing the cytoplasmic side of the organelle membrane. In this study, 19 of 27 Na and

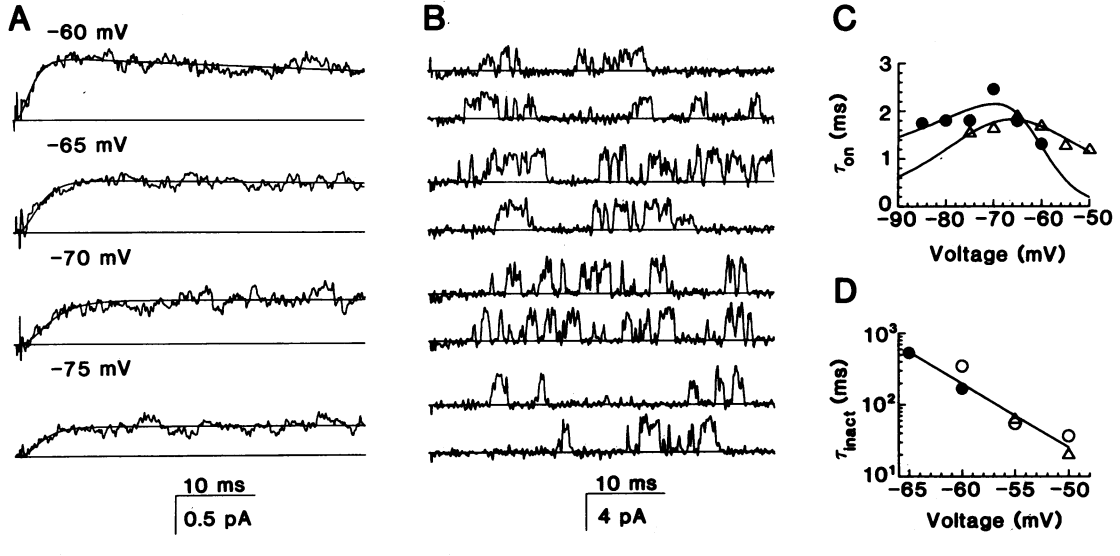

FIG. 4. Voltage-step activation of a K channel. (*A*) The channel was deactivated by holding the bilayer voltage at −100 mV and then activated by voltage steps to the potentials indicated (45-msec step duration, 0.5-Hz rate; symmetric 500 mM KOAc; the records were inverted for easier comparison with traditional macroscopic K currents). The records shown are the ensemble averages of either 160 (records at −60 and −70 mV) or 240 (records at −65 and −75 mV) voltage steps, from which averaged blank records (no channel activity) at each potential have been subtracted. Records were filtered (low pass) at 2.5 kHz. Before subtraction, the noise in the blank records was reduced by replacement of each averaged record with a spline function fitted to the averaged trace. The time required for charging the bilayer capacitance was reduced by switching to a low-gain feedback resistor (50 MΩ) 1 msec before the voltage step and then switching back to a high-gain feedback resistor (50 GΩ) 25 μsec after the beginning of the step. The onset of the pseudomacroscopic record is sigmoidal, and there is some inactivation at the more depolarized potentials. The smooth curves are fits of a Hodgkin–Huxley type model (23) of activation (n^4), multiplied by a decaying single exponential. (*B*) Representative pairs of single-channel records from the ensembles used in calculation of the corresponding average currents for the voltages shown in *A* (filtered at 2.5 kHz). (*C*) The time constants of activation for two experiments (data from records in *A* are solid circles) are plotted as a function of membrane potential. The curves are fits of the predicted time constants, calculated as the reciprocal of the sum of single voltage-dependent opening and closing rates. (*D*) The time constants of inactivation for three experiments (data from records in *A* are solid circles; other symbols denote separate experiments), estimated by fitting the decay of the average currents by a single exponential decaying toward zero, are plotted as a function of membrane potential.

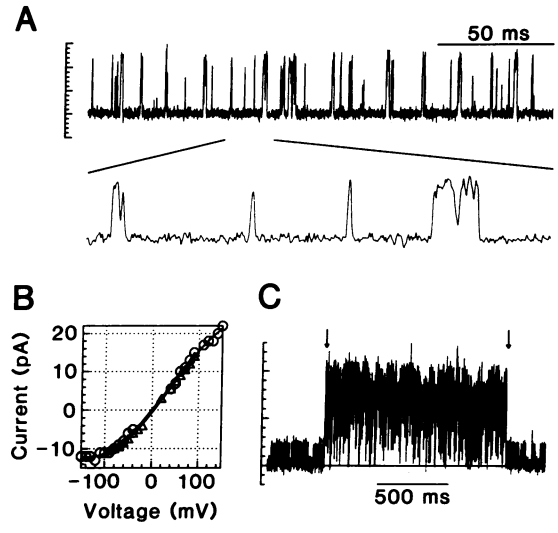

FIG. 5. Large-conductance K channel. (*A*) Upper record: A single K channel at +70 mV (symmetric 500 mM KOAc; large tic interval is 5 pA). Channel openings are brief, flickering openings that are difficult to resolve, even at a wide bandwidth (here, ≈5 kHz). This channel is much more active than usual. Lower record: A 20-msec segment of the upper record is shown on an expanded time scale. (*B*) The single-channel *I–V* relations measured in symmetric 500 mM K^+ solutions were approximately linear near 0 mV but exhibited a voltage-dependent decrease in slope on increasing polarization. The decrease in slope conductance is most marked at negative potentials for one of the channels shown, but the orientation of the channel is not certain. The slope conductance of both of these channels, measured at 0 mV, is ≈150 pS. (*C*) High-activity mode of a large-conductance K channel held at −40 mV. A small-conductance K channel is active throughout the record, adding to the apparent background noise. The large-conductance channel was at first relatively inactive (low-activity brief openings not captured in this record), then switched to a high-activity mode (first arrow), and finally returned to its low-activity mode (second arrow).

delayed rectifier K channels incorporated with their cytoplasmic end facing the chamber to which the organelles were added, which is the orientation predicted above. From the binomial distribution, the probability of observing 19 or more channels facing the same direction, if the orientation were random, would be 0.026. The orientation of large conductance K channels could not be determined because of their lack of voltage-dependent gating or rectification. Axoplasmic organelles may also have provided the channels incorporated from cut open squid axon in a previous study (28).

K channels have been observed in axosomes (20- to 200-μm-diameter intraaxonal vesicles) formed by an unidentified Ca-dependent process after damage to the axolemma (29). It seems unlikely that the channels we observed were from the intracellular membranes that form axosomes because the formation of axosomes cannot be stimulated in extruded axoplasm, although vesiculation prior to extrusion cannot be ruled out (H. Fishman, personal communication).

The properties of voltage-dependent gating and permeation of the Na channels from axoplasm were sufficiently similar to those of squid axolemmal Na channels for us to surmise that the voltage-gated Na channel might be transported in axoplasmic organelles in its native state. The two types of axoplasmic K channels, on the other hand, appear similar to two classes of axolemmal K channels in their dephosphorylated state, suggesting that the K channels in organelles might be transported in organelles in an unphosphorylated state. The physiological function of the phosphorylation of these K channels is not known, although it has been suggested that it might serve as a signal for either retention or removal of the protein from the axolemma (21). Because we could not determine the direction of transport of the organelles we studied—i.e., toward the axolemma or toward the cell bodies—we do not know whether the Na and K channels acquired the physiological properties we observed before or after insertion into the axolemma. Our demonstration of physiologically active plasma membrane ion channels in cytoplasmic transport organelles is a first step toward study of a broader range of organelle types, such as are present in the cell bodies of cultured neurons, which might provide further insight into the physiological development of these channels during their processing in organelles.

The authors would like to thank Drs. W. K. Stell, W. Giles, D. Weinreich, and B. K. Krueger for their comments on an earlier draft of this manuscript. We are also grateful to Dr. E. Perozo for providing prepublication copies of his manuscripts, and Drs. E. Perozo and F. Bezanilla for helpful discussions. We thank Dr. John Daly, National Institute of Diabetes and Digestive and Kidney Diseases (Bethesda), for his generous gift of BTX. This research was initiated with the support of a Grass Foundation Fellowship to W.F.W. and was also supported by an operating grant from the Medical Research Council of Canada (Grant MA-10053) and an Implementation Grant from the Alberta Heritage Foundation for Medical Research (AHFMR). W.F.W. is an AHFMR Fellow and R.J.F. is an AHFMR Scholar.

1. Hille, B. (1984) *Ionic Channels of Excitable Membranes* (Sinauer, Sunderland, MA).
2. Alberts, B., Bray, D., Lewis, J., Raft, M., Roberts, K. & Watson, J. D. (1989) *Molecular Biology of the Cell* (Garland, New York).
3. Catterall, W. A. (1988) *Science* **242**, 50–61.
4. Young, J. Z. (1936) *Q. J. Microsc. Sci.* **78**, 367–386.
5. Grafstein, B. & Forman, D. S. (1980) *Physiol. Rev.* **60**, 1167–1283.
6. Villegas, G. M. & Villegas, R. (1984) *Curr. Top. Membr. Trans.* **22**, 3–37.
7. Brismar, T. & Gilly, W. F. (1987) *Proc. Natl. Acad. Sci. USA* **84**, 1459–1463.
8. Vale, R. D., Schnapp, B. J., Reese, T. S. & Sheetz, M. P. (1985) *Cell* **40**, 449–454.
9. Schroer, T. A., Schnapp, B. J., Reese, T. S. & Sheetz, M. P. (1988) *J. Cell Biol.* **107**, 1785–1792.
10. Baker, P. F., Hodgkin, A. L. & Shaw, T. I. (1962) *J. Physiol. (London)* **180**, 424–438.
11. Wonderlin, W. F., Finkel, A. & French, R. J. (1990) *Biophys. J.* **58**, 289–297.
12. Plonsey, R. (1969) *Bioelectric Phenomena* (McGraw-Hill, New York), p. 57.
13. Brown, A. & Lasek, R. J. (1990) in *Squid as Experimental Animals*, eds. Gilbert, D. L., Adelman, W. J., Jr., & Arnold, J. M. (Plenum, New York), pp. 235–302.
14. Behrens, M. I., Oberhauser, A., Bezanilla, F. & Latorre, R. (1989) *J. Gen. Physiol.* **93**, 23–41.
15. Correa, A. M. & Bezanilla, F. (1988) *Biophys. J.* **53**, 226 (abstr.).
16. Llano, I., Webb, C. K. & Bezanilla, F. (1988) *J. Gen. Physiol.* **92**, 179–196.
17. Conti, F. & Neher, E. (1980) *Nature (London)* **285**, 140–143.
18. Llano, I. & Bookman, R. J. (1986) *J. Gen. Physiol.* **88**, 543–569.
19. Gilbert, D. L. & Ehrenstein, G. (1969) *Biophys. J.* **9**, 447–463.
20. Perozo, E., Bezanilla, F. & Dipolo, R. (1989) *J. Gen. Physiol.* **93**, 1195–1218.
21. Augustine, C. K. & Bezanilla, F. (1990) *J. Gen. Physiol.* **95**, 245–271.
22. Perozo, E., Jong, D. S. & Bezanilla, F. (1991) *J. Gen. Physiol.*, in press.
23. Hodgkin, A. L. & Huxley, A. F. (1952) *J. Physiol. (London)* **117**, 500–544.
24. Clay, J. (1989) *Biophys. J.* **55**, 407–414.
25. Perozo, E., Vandenberg, C. A., Jong, D. S. & Bezanilla, F. (1991) *J. Gen. Physiol.*, in press.
26. Mahar, J., Lukacs, G. L., Li, Y., Hall, S. & Moczydlowski, E. (1991) *Toxicon* **29**, 53–71.
27. Schmidt, J., Rossie, S. & Catterall, W. A. (1985) *Proc. Natl. Acad. Sci. USA* **82**, 4847–4851.
28. Torres, R. M., Coronado, R. & Bezanilla, F. (1984) *Biophys. J.* **45**, 38 (abstr.).
29. Fishman, H. M., Tewari, K. P. & Stein, P. G. (1990) *Biochim. Biophys. Acta* **1023**, 421–435.